Astron. Astrophys. 348, 685–692 (1999)

ASTRONOMY AND ASTROPHYSICS

HI spatial distribution in the galaxy NGC 3783

J.A. García-Barreto[1], **F. Combes**[2], **B. Koribalski**[3], **and J. Franco**[1]

[1] Instituto de Astronomía, Universidad Nacional Autónoma de México, Apartado Postal 70–264, México D.F. 04510, México
[2] DEMIRM, Observatoire de Paris, 61 Av. de l'Observatoire, F-75014 Paris, France
[3] Australia Telescope National Facility, CSIRO, P.O. Box 76, Epping, NSW 2121, Australia

Received 14 April 1999 / Accepted 29 June 1999

Abstract. We have mapped the emission from atomic hydrogen at λ=21 cm from the galaxy NGC 3783 with the Australia Telescope Compact Array. Our main results are: **a)** the HI morphology is irregular and perturbed, gathered in three blobs apparently unrelated to the optical morphology; **b)** the observed HI velocity distribution indicates a normal disk in differential rotation with a constant velocity out to a radius of 160″ (30 kpc), **c)** the inclination of the disk is about 25° with the kinematic major axis at a position angle slightly different from that of the stellar bar, **d)** the HI mass inside a radius of 18″ is only 2.1×10^7 $M_\odot$, the total HI mass within 180″ is 1.1×10^9 $M_\odot$ and the dynamical mass is 2×10^{11} $M_\odot$. The bulk of the gas in NGC 3783 is outside the diameter of the stellar bar; **e)** Numerical simulations of the gas flow in the barred potential derived from the red image indicate that the pattern speed is Ω_p = 38 km/s/kpc: the ring of Hα emitting regions encircling the bar would then correspond to UHR, and the Hα accumulation in the center to a nuclear ring. Various possibilities are discussed to account for the active nucleus fuelling.

Key words: galaxies: active – galaxies: general – galaxies: individual: NGC 3783 – galaxies: kinematics and dynamics – galaxies: spiral

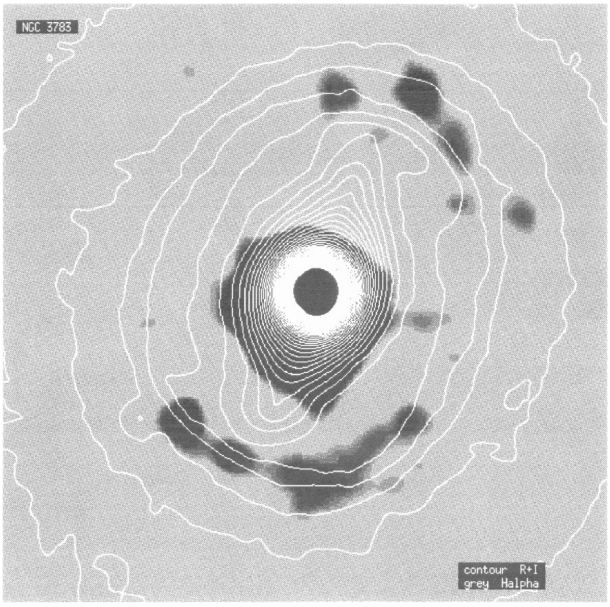

Fig. 1. Optical emission of the innermost continuum light of NGC 3783 in the R plus I broadband filters (in contours) superimposed on the continuum-free Hα+[NII] emission (in grey scale) from García-Barreto et al. (1996). North is up, East is to the left. Angular scale is such that distance from peak to peak Hα emission outside the bar from the south east to the north west is about 37″.

1. Introduction

The activity observed in the nucleus of Seyfert 1 galaxies requires gas fuelling, either constant or episodic, of a few tenths to a few $M_\odot$ yr^{-1} for a significant period of time. Some authors have suggested as a likely possibility that fuelling may be a direct consequence of a stellar bar (Simkin, et al. 1980; Shlosman et al. 1989) which causes radial motions of gas in the disk of the surrounding spiral galaxy. Therefore it is important to determine the total amount of neutral hydrogen (HI) gas, its spatial distribution and the rotation curve.

NGC 3783, a Seyfert 1 SBa galaxy, shows a broad Hα line and lines of high ionization atoms (Pelat et al. 1981; Atwood et al. 1982; Evans 1988; Winge et al. 1992, George et al. 1995). The optical structure of NGC 3783 has a diameter of $1'.9 \times 1'.7$ at an inclination angle of $i = 23°$ with a bright compact nucleus, a stellar bar at a position angle of $PA_{\rm b} \approx 163°$ and radius $r_{\rm b} = 18''$ (Mulchaey et al. 1997), a bright inner ring just outside of the stellar bar and small pitch angle spiral arms (Kennicutt 1981).

The peak to peak distances from the nucleus to the HII regions to the NW and SE are $\sim 21''$ and $\sim 16''$, respectively, (see Fig. 1). Hα emission has been detected from the innermost central region, from regions just at the end of the stellar bar and from regions perpendicular to the bar (Forte et al. 1987; Winge et al. 1992; García-Barreto et al. 1996 and Fig. 1). The nucleus of NGC 3783 is a strong X-ray emitter in the 2–10 keV band (Piccinotti et al. 1982) and in the 0.2–3.5 keV band (Fabbiano et al. 1992). The short time scale variability of its optical, X-ray and UV continua suggests a collimation outflow from NGC 3783 (Reichert et al. 1994; Stirpe et al. 1994; Alloin et al. 1995). Ra-

Send offprint requests to: J.A. García-Barreto
(tony@astroscu.unam.mx)

dio continuum emission has been detected from an unresolved central source at different frequencies indicating an optically thin synchrotron emission (Ulvestad & Wilson 1984; Alloin et al. 1995). Its far infrared (FIR) IRAS fluxes are $f_{60\mu} \approx 3.37$ Jy and $f_{100\mu} \approx 5.12$ Jy with a two color dust temperature of $T_{\rm d} \approx 39$ K. In this paper we adopt a distance to NGC 3783 as 38.5 Mpc, $H_0 = 75\,{\rm km\,s^{-1}\,Mpc^{-1}}$, as given by Tully (1988). The FIR luminosity is $L_{\rm FIR} \approx 3.1 \times 10^{43}$ ergs s^{-1} (according to the formula by Helou et al. 1985). Spectroscopic studies reveal extremely broad Balmer lines with a full width at zero intensity (FWZI) of the Hα line of $\approx 7,300 \rightarrow 10,000\,{\rm km\,s^{-1}}$ (Pelat et al. 1981; Evans 1988). Broad line components are increasingly blue-shifted relative to the systemic velocity (Evans 1988). The density, ionization parameter, and velocity dispersion of the emitting clouds increase toward the central ionizing source (Pelat et al. 1981; Atwood et al. 1982; Evans 1988; Winge et al. 1992). The optical systemic velocity using lines of OI, OII and NII is $v_{\rm sys}^{\rm opt} \approx 2930\,{\rm km\,s^{-1}}$ (Pelat et al. 1981), while the average velocity of the narrow line region is 2890 km s^{-1}.

Single dish observations of NGC 3783 indicate a total HI mass of $M_{\rm HI} = 3.6 \times 10^9$ M$_\odot$, and a systemic velocity of $v_{\rm sys} \approx 2902\,{\rm km\,s^{-1}}$ (Huchtmeier & Richter 1989). A previous interferometric study of the dynamics and spatial distribution of neutral hydrogen in NGC 3783 indicated that the total HI has an extent similar to the weak surface brightness optical contours ($25 \rightarrow$ 28 mag arcsec^{-2}), and that the velocity field exhibits irregular structures (Simkin & van Gorkom 1984).

The present study focuses on the spatial distribution of the HI gas in NGC 3783 obtained with the Australia Telescope Compact Array (ATCA), giving an angular resolution of 30″ and a spectral resolution of 6.7 km s^{-1}. In Sect. 2 we describe the HI observations. In Sect. 3 we describe the HI spatial distribution and velocity field, discuss possible physical scenarios for the central gas kinematics in NGC 3783, and describe the central radio continuum emission. The dynamics of the central parts is investigated through numerical simulations fitted to the observations in Sect. 4. Our conclusions are summarized in Sect. 5.

2. Observations and data reduction

The observations of NGC 3783 were carried out with the 1.5A configuration of ATCA in Narrabri, NSW, on 1996 October 18, in the 21-cm neutral hydrogen line and the 13-cm radio continuum. The two intermediate frequency (IF) bands were centered at 1407 and 2378 MHz with a total bandwidth of 8 and 128 MHz, respectively. The total time on source was ∼9 hours. The pointing center was α(J2000) = $11^{\rm h}\,39^{\rm m}\,01^{\rm s}.8$ and δ(J2000) = $-37^\circ\,45'\,20''$, which is about 1′ away from the center of NGC 3783.

The initial calibration, data editing and final analysis were performed using the AIPS package. For both frequencies PKS 1934–638 (14.893 Jy / 11.553 Jy) was used as flux calibrator, PKS 1151–348 (6.0 Jy / 4.6 Jy) and PKS 1215–457 (4.8 Jy / 3.6 Jy) as phase calibrators, and both PKS 1934–638 and PKS 0823–500 (5.8 Jy / 5.8 Jy) as bandpass calibrators.

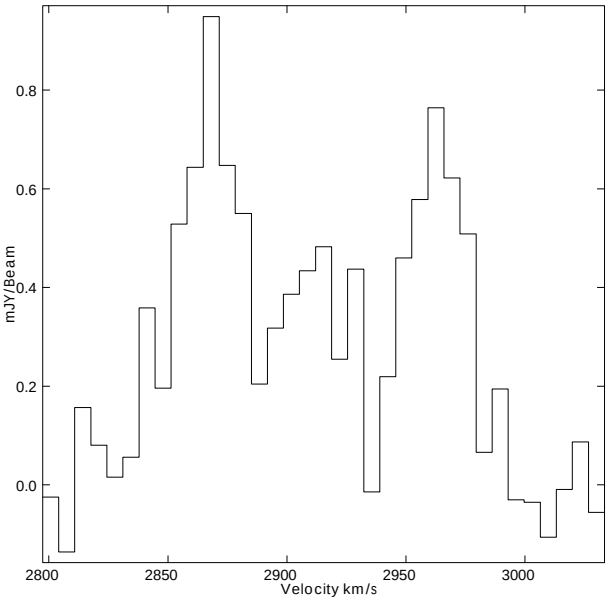

Fig. 2. HI spectrum of NGC 3783. Only 23 of the 35 channels show emission in the velocity interval from 2840 to 2990 km s^{-1}.

2.1. HI observations

The bandwidth of the first IF was divided into 512 channels spaced by 15.625 kHz (or 3.37 km s^{-1}) and covered a velocity range from about 2000 to 3600 km s^{-1}. The line-free channels were averaged and subtracted using the AIPS task UVLSF.

The resulting line data were Fourier transformed using 'natural weighting' to produce a cube with dimensions 256 pixel × 256 pixel × 35 channels with 8″ pixels and a final channel separation of 6.74 km s^{-1}. The data showed emission in the velocity range from ∼2840 to 2990 km s^{-1}. Each of the 35 channels was CLEANed and restored with a clean beam of 45″ (FWHM) in order to detect extended emission. The rms noise per channel was ∼1.7 mJy beam^{-1}. Only 23 out of the 35 cleaned channels show HI emission (see Fig. 2). The integrated neutral hydrogen distribution and the corresponding velocity field were derived from the data by moment analysis using the AIPS task MOMNT. We smoothed the data both in velocity and space using Hanning (3 channels) and Boxcar (7 pixels) functions, respectively. Only fluxes greater than 2 mJy beam^{-1} were included in the integration.

2.2. Radio continuum observations

The narrow-band 20-cm continuum data were Fourier transformed using 'uniform weighting' to produce a cube with dimensions 1024 pixel × 1024 pixel with 2″ pixels. It was CLEANed and restored with a clean beam of 13.″5 (FWHM). The rms noise was about 0.12 mJy beam^{-1}. The bandwidth of the second IF was divided into 32 channels; the central 26 of those were averaged to form the 13-cm radio continuum image. The data were Fourier transformed using 'uniform weighting' to produce a cube with dimensions 1024 pixel × 1024 pixel with

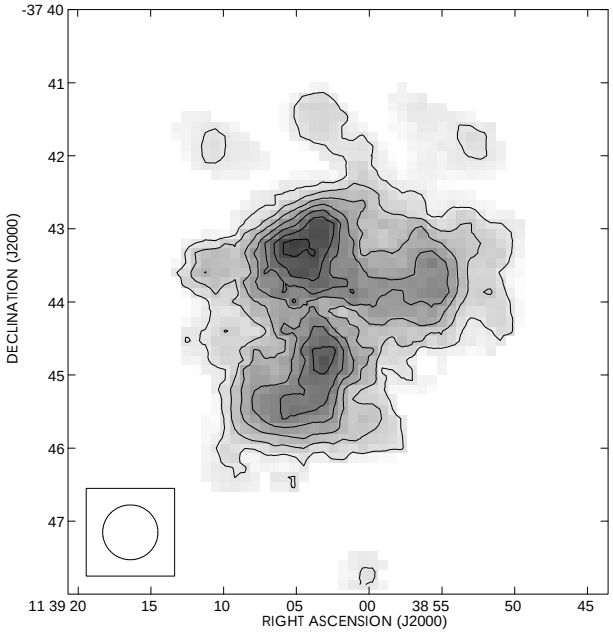

Fig. 3. Integrated neutral hydrogen distribution (zero moment) of NGC 3783. The contour levels are 0.05, 0.1, 0.15, 0.2, 0.25, 0.3, and 0.35 Jy beam^{-1} km s^{-1}. The first contour corresponds to an HI column density of 6.25×10^{19} atoms cm^{-2}. The synthesised beam (45″) is indicated in the lower left corner. North is to the top, east to the left.

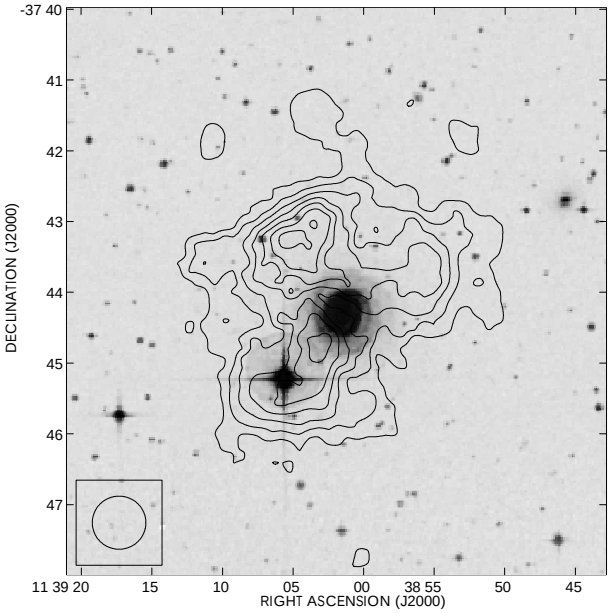

Fig. 4. Integrated neutral hydrogen distribution of NGC 3783 (in contours) superimposed on the innermost continuum light emission from a POSS plate (in grey scale). The optical emission at low levels (25 mag arcsec^{-2}) extends to about 60″ to the south-west and about 120″ elsewhere.

2″ pixels. It was CLEANed and restored with a clean beam of (FWHM). The rms noise was 0.06 mJy beam^{-1}.

3. Results and discussion

3.1. HI emission

The spatial distribution of HI in NGC 3783 is shown in Figs. 3 and 4. The map results from integrating the column density over the velocity range with HI emission. Fig. 5 shows the spatial distribution of HI in individual channel maps. The overall spatial distribution of the HI emission is that of a disk with the blue-shifted velocity to the NW, and the red-shifted velocity to the SE.

The integrated flux density inside a radius of 180″ (34 kpc) is $F_{\rm HI}$ = 3.2 Jy km s^{-1}. This value is a factor of 3 lower than the single dish value of 10.3 Jy km s^{-1} (Huchtmeier & Richter 1989). This difference is most likely a result of missing short spacings and our column density threshold of $N_{\rm HI} = 6 \times 10^{19}$ atoms cm^{-2}. More extended emission could be present in the galaxy at much lower levels. From our observations, the total HI mass inside a radius of 180″ is $M_{\rm HI} \approx 1.1 \times 10^9$ M$_\odot$. The HI mass inside the stellar bar radius of 18″ (3.4 kpc) is only $\approx 2.1 \times 10^7$ M$_\odot$, i.e. 2% of the total mass. The HI integrated column density map indicates that most of the neutral atomic gas is distributed outside the stellar bar with large concentrations up to 120″ (22.5 kpc) away from the nucleus to the NE, NW and SE of the galaxy (see Fig. 4). The HI extent to the SW is only about 60″ (11.2 kpc). The kinematical center was found to be at α(J2000) = $11^{\rm h}\,39^{\rm m}\,01^{\rm s}.74$ and δ(J2000) = $-37^\circ\,44'\,20''.2$.

The rotation velocity, $v_{\rm rot}$, and the position angle, PA, of the line of nodes (major axis) were obtained by fitting the velocity field in inclined annuli using the AIPS program GAL. The kinematic major axis of the HI distribution is at $PA \approx 145 \pm 2^\circ$. This angle differs by about 15° from the PA of the bright stellar bar which is at $\approx 163^\circ$ (García-Barreto et al. 1996; Mulchaey, Regan & Kundu 1997). The kinematic minor axis of NGC 3783 is thus at $PA \approx 55^\circ$ indicating that the regions NE and SW of the galaxy are at velocities near the systemic velocity of the galaxy.

Fig. 6 shows the observed rotation velocity, while Fig. 7 presents the velocity field. The fitted systemic velocity is $v_{\rm sys} \approx 2910 \pm 5$ km s^{-1}. The observed velocities show an average rotational velocity of 160 km s^{-1}, with a maximum of about 170 km s^{-1}, and then a trend of decreasing velocity down to about 130 km s^{-1} at radii between 60″ to 70″. Then increasing velocities up to 160 km s^{-1} at radii between 90″ to 100″, showing a rotation curve similar to other spiral galaxies and our Galaxy (see Fig. 6 of Giovanelli & Haynes 1988). The total dynamical mass inside a radius of 180″ is $M_{\rm dyn} \approx 2 \times 10^{11}$ M$_\odot$, for an inclination of $i = 25^\circ$ and a constant rotation velocity of 160 km s^{-1}.

The spatial distribution of HI and its velocity field indicate gas rotating in a disk. Since there is little HI in the stellar bar, and the optical image does not have bright spiral arms, it is difficult to assign any correspondence between the optical features (nucleus, bar, arms) and the HI distribution.

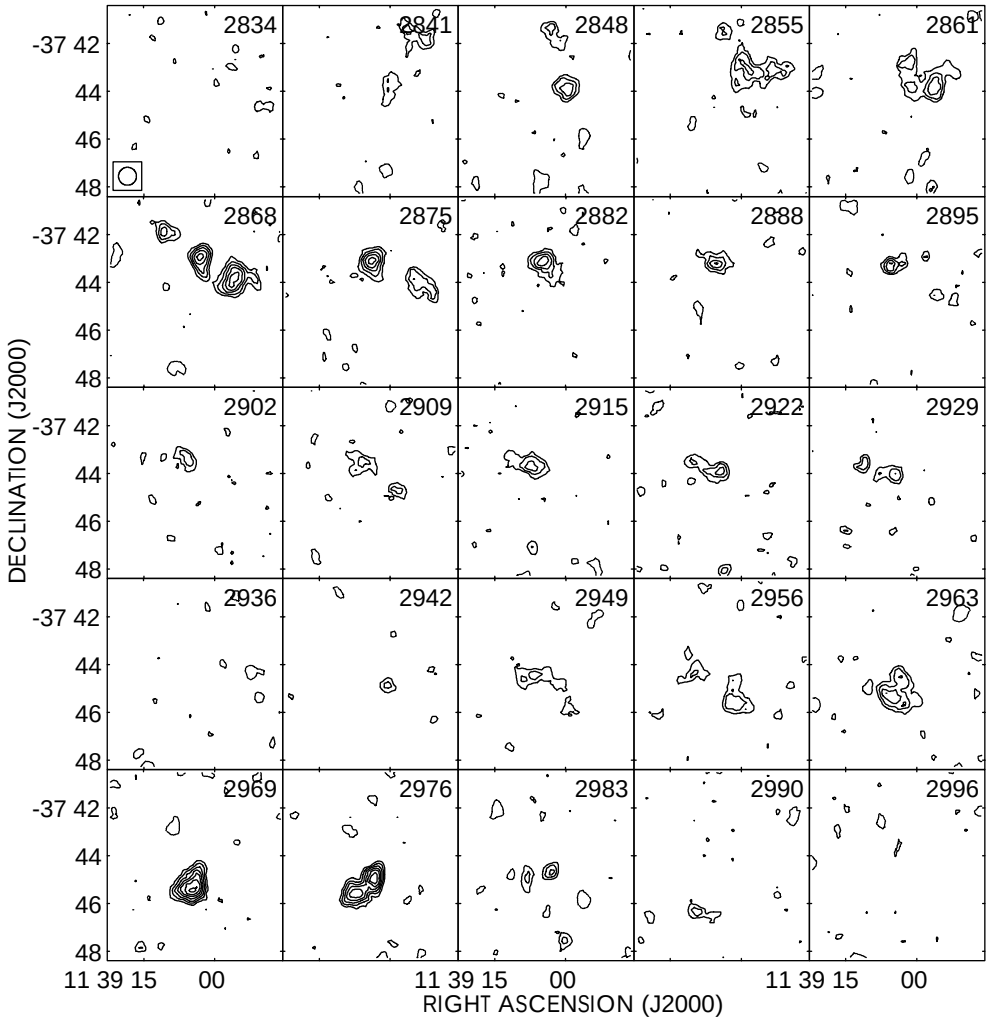

Fig. 5. HI channel maps of NGC 3783. Contour levels are –4, 4, 6, 8, 10, 12, 14 and 16 mJy beam^{-1}. The restoring beam is 45″.

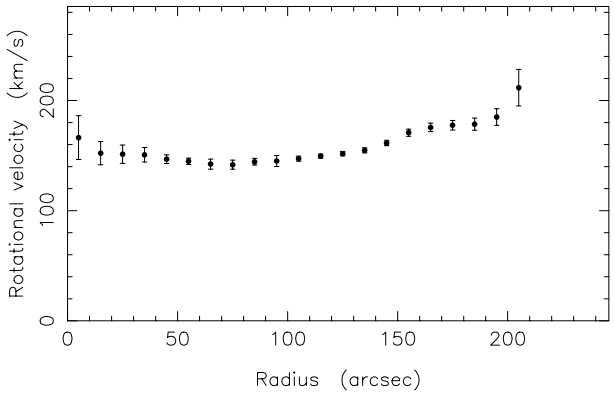

Fig. 6. Rotation velocity as a function of radius including both the receding and approaching sides of the galaxy.

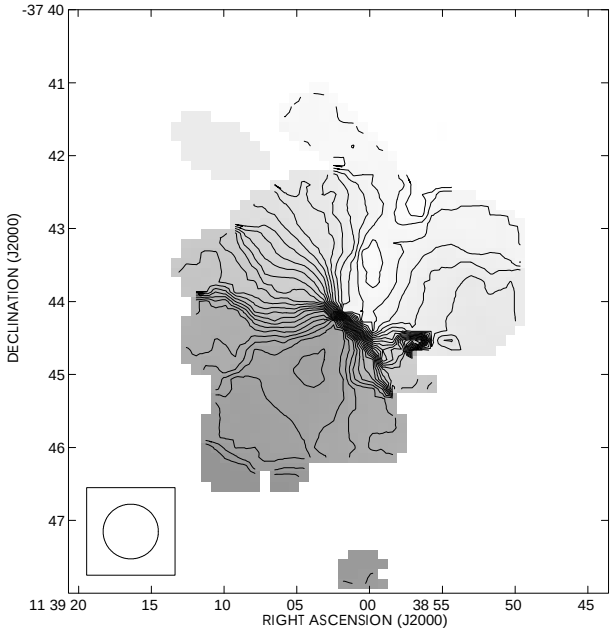

Fig. 7. Intensity weighted mean velocity field (first moment) of NGC 3783. The contour levels go from 2845 to 2990, step 5 km s^{-1}.

3.2. Origin of the gas in the central region

The activity observed in the nucleus of NGC 3783 requires gas fuelling. One likely possibility for gas to be present in the inner few arcseconds is inflow from the disk. In terms of galactic dynamics, this could be achieved by any combination of processes leading to angular momentum exchange in the disk of

the host galaxy (Lynden-Bell & Kalnajs 1972; Lynden-Bell & Pringle 1974; Phinney 1994). Possibilities are: inflow associated with the presence of a non-axisymmetric potential (e.g Athanassoula 1992; Friedli & Benz 1993; Habe & Wada 1993; Friedli & Martinet 1997), inflow due to the perturbations exerted by ram pressure from intergalactic gas (Kritsuk 1983), inflow due to tidal or direct interactions with a nearby companion (e.g. Toomre 1978; Noguchi 1988; Salo 1991; Horellou & Combes 1993), and inflow due to accretion of cooling flows (Fabbiano et al. 1989).

Considering first the possibility of a companion, there is only one candidate seen in the optical images. A small galaxy at α(J2000) = $11^{\rm h}\,38^{\rm m}\,45^{\rm s}.62$ and δ(J2000) = $-37^\circ\,42'\,40''.9$ with an approximate apparent diameter of $35''$ lies $\sim 3'.6$ to the NW of NGC 3783 (visible in Fig. 4). We have not detected any HI at this position, within our velocity range from 2000 to 3600 km s^{-1}. Since nothing is known about this galaxy in terms of its redshift or distance, and since it does not show any apparent signs of tidal interaction with NGC 3783, we may assume that it is a background object. Since the distribution of HI around NGC 3783 is very irregular, and appears un-relaxed, a likely possibility then is that it has swallowed recently an HI-rich companion; this would explain the nuclear activity. However, we have no way to confirm this hypothesis. In the absence of nearby large optical companions, or optical signs of tidal interactions, we will assume in the following that gas responds only to the action of a non-axisymmetric gravitational potential. The direction of the bar torques on the gas depend strongly on the location of the resonances, and therefore on the bar pattern speed (see e.g. Combes 1988). To infer this parameter from observations, we have performed numerical simulations and they are presented in Sect. 4.

3.3. Radio continuum emission

The radio continuum images show a central source in NGC 3783, at α(J2000) = $11^{\rm h}\,39^{\rm m}\,01^{\rm s}.63$ and δ(J2000) = $-37^\circ\,44'\,20''.0$, with peak flux densities of 27.8 mJy beam^{-1} at 20-cm, 19.5 mJy beam^{-1} at 13-cm, and faint emission surrounding the nucleus. The total flux densities at 20- and 13-cm are about 36.0 and 30.4 mJy, respectively.

The radio continuum emission from the disk that is related with star formation and evolution suggests in NGC 3783, based in the weak Hα fluxes in the NW and SE outside the stellar bar radio continuum fluxes of the order of few tenths of μJy, well below the current detectability with reasonable integration times.

The spectral index between 1407 MHz and 2378 MHz is $\alpha \approx -0.8$. Previous high resolution continuum observations showed an unresolved source with a peak flux density of 32.7 mJy beam^{-1} at 1.4 GHz (Alloin et al. 1995), 13 mJy beam^{-1} at 4.8 GHz (Ulvestad & Wilson 1984), 6.1 mJy beam^{-1} at 8.4 GHz, and 2.6 mJy beam^{-1} at 14.9 GHz (Alloin et al. 1995).

Our continuuum maps confirm the non-existence of nuclear extended emission from NGC 3783 (e.g., radio lobes). In general, Sy 1's are predominantly less luminous than Sy 2's galaxies (de Bruyn & Wilson 1978; Ulvestad & Wilson 1984; Baum et al. 1993), the thermal contribution is negligible in the broad-line region (Ulvestad et al. 1981), and the radio continuum is mostly non-thermal (de Bruyn & Wilson 1978). The detected radio continuum radiation from the central region coincides with the distribution of the central Hα emission, but our observations cannot identify the physical origin of the emission: either star formation and its subsequent evolution in circumnuclear regions (e.g. Terlevich et al. 1992, 1994; see review by Dultzin-Hacyan 1997) or activity from the nucleus of the galaxy. The spectral index of the radio continuum emission in NGC 3783 indicates that the radiation is optically thin synchrotron emission. The power at 20 cm is only $P_{20\rm cm} = 4.6 \times 10^{20}$ W Hz^{-1}.

4. Numerical simulations

In order to gain more insight in the NGC 3783 galaxy dynamics, we compute the response of gas test-particles in the potential created essentially by the stars, (e.g. García-Burillo et al. 1994; Sempere et al. 1995). A realistic galaxy potential has been derived from the red band image. We assume that the barred disk can be fitted by a single and well-defined wave pattern, characterized by the pattern speed Ω_p. Since the periodic orbits, and the consequent gas behaviour, strongly depend on Ω_p, the observed morphology of the gaseous and stellar disks will only be recovered with a narrow range of pattern speeds. The method has been shown to be very sensitive to this parameter (e.g. García-Burillo et al. 1993).

4.1. Method

The gravitational potential is obtained from Fig. 1 in the following way. The image is first deprojected using an inclination of 25°, and a PA of 145° (cf Sect. 3). The resulting image is then Fourier transformed on a 2D grid of 256x256. The image used extends up to a maximum radius of 5.8kpc, since the signal-to-noise decreases outwards. The spatial resolution is therefore of the order of the cell size, i.e. 45 pc. Outside our maximum radius, the potential is extended analytically, in an axisymmetric manner, and in order to have a flat rotation curve. Fig. 8 shows the resulting rotation curve, assuming a constant mass-to-light ratio. The figure includes the data points from the HI observations. A constant M/L allows to fit the observations; only in the very center, inside a radius of 300 pc (or $1.6''$), we have reduced the M/L ratio to avoid the high luminosity peak due to the Seyfert nucleus (but the involved mass is negligible). The constant M/L ratio that inside a radius of 5.8 kpc give a total mass of 2.5 10^{10} M$_\odot$.

The gravitational potential is thus obtained in the plane, but we perform the gas simulations in 3D assuming cylindrical symmetry for the gravitational forces within the plane. This hypothesis is justified considering that the gas thickness (H$_{gas}$ ∼50–100pc) is much smaller than the stellar thickness (H$_{stars}$ ∼1 kpc). We assume H$_{stars}$ to be constant with radius. The vertical z-forces are derived assuming an isothermal stellar disk with a sech^2(z/H) density law.

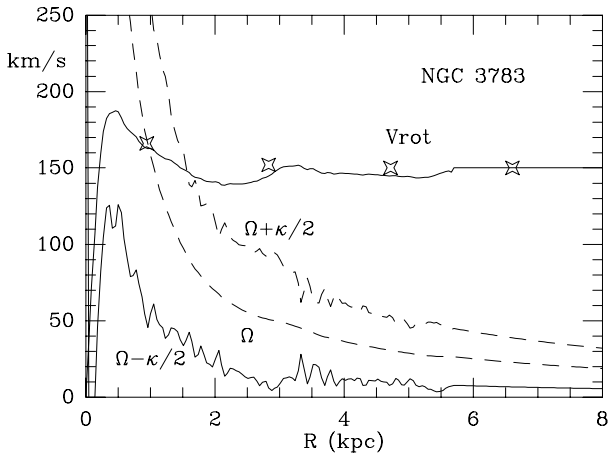

Fig. 8. Rotation curve obtained from the galaxy potential, derived from the red image, and adopted for the simulations. The stars are the data points derived from the HI observations. Also displayed are the derived principal resonance frequencies Ω, Ω-κ/2 and Ω+κ/2.

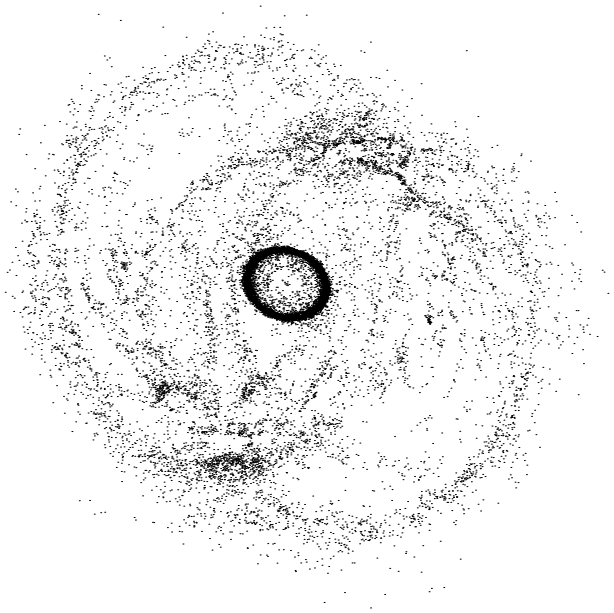

Fig. 9. Particle plots of the Ω_p = 50 km/s/kpc run, at steady-state. This corresponds to a corotation at 2.5 kpc, and an outer Lindblad resonance in the disk at 5 kpc. The particles are thus driven out to the OLR, which does not fit the observed morphology.

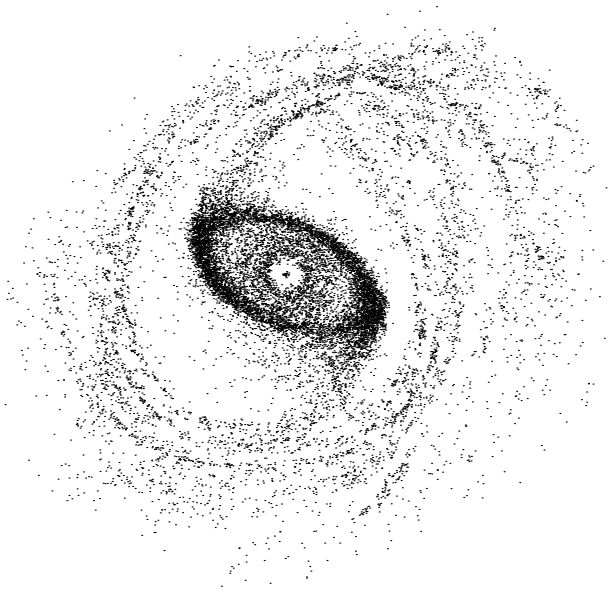

Fig. 10. Particle plots of the Ω_p = 26 km/s/kpc run at steady-state. The pattern speed is so low that there are two well-defined ILRs, and the response in the region between the two ILRs is perpendicular to the bar, which does not fit the observations.

Once the potential is computed, we separate the axisymmetric part from the non-axisymmetric one. The gaseous disk is set-up initially with circular orbits in rotational equilibrium in the axisymmetric potential. Progressively, with a time-scale of 250 Myr, the non-axisymmetric part is introduced with a fixed angular speed Ω_p. The simulations are continued until a steady response of the gas is reached, which appears after $\sim$ 400-500 Myr. We have computed several runs, varying the value of Ω_p, until a morphology compatible with the observations has been obtained.

We have not considered here the self-gravity of the gas, since its mass inside the optical disk is not dominant and self-gravity will only introduce small morphological perturbations (Sempere et al. 1995). We have also adopted a simple collisional scheme for gas clouds, without a cloud mass spectrum (Combes & Gerin 1985). Clouds interact with each other via inelastic collisions, losing 75% of their radial relative velocity in the collision. The clouds initially have an exponential radial distribution, with a scale length of 1.5 kpc (8″).

4.2. Results

Reproducing exactly the outer spiral has not been considered as a strong constraint, because it is beyond the radius where the red image is used; yet a spiral structure forms, generated by the bar pattern, and rather similar to the observed one.

The simulations run with different values of Ω_p, between 20 and 60 km/s/kpc. When the pattern speed is high, the outer Lindblad resonance moves in the visible disk, and the matter accumulates near the OLR in a ring elongated perpendicular to the bar (Fig. 9). For lower values of Ω_p, the radius of corotation moves towards the outer parts, and there are two well separated inner Lindblad resonances. In between them, there is a large region where the perpendicular orbits x_2 dominate, generating a response perpendicular to the stellar bar in the center, which is not observed (Fig. 10). Note that the presence of the two ILRs cannot be inferred directly from the $\Omega - \kappa/2$ curve, since the bar is strong, and the potential is non-axisymmetric. The best fit with observations is obtained for Ω_p = 38 km/s/kpc; the corotation is then at 4.5 kpc, and we obtain an inner ring near the UHR, at about the position of the observed Hα ring. The choice of Ω_p is therefore constrained to a narrow range around 38 km/s/kpc (Fig. 11).

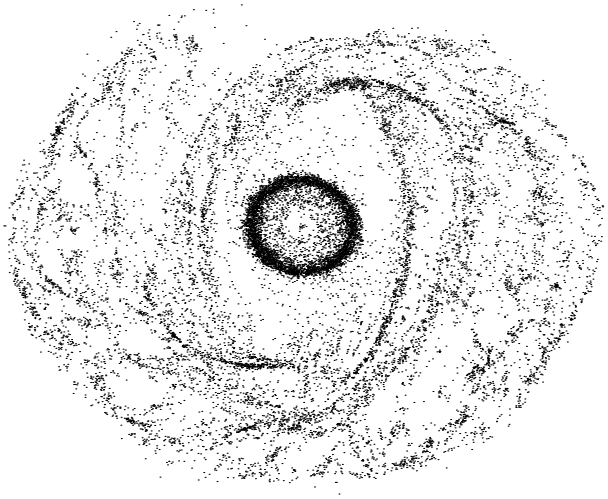

Fig. 11. Particle plots of the run with a bar pattern speed of Ω_p = 38 km/s/kpc. There is an inner ring at UHR, which corresponds to the Hα ring at $\sim$ 3 kpc radius, but also a nuclear ring of radius 0.75 kpc.

4.3. Discussion

Angular momentum transfer is required to bring gas to the central regions in barred galaxies (García-Burillo et al. 1993, 1994, Sempere et al. 1995; Lindblad & Kristen 1996; Lindblad et al. 1996; Sellwood & Debattista 1996). The bar torques are able to drive gas from the corotation radius to the center if there is no inner Lindblad resonance, or to make the gas pile up near the ILR. The simulations indicate that the most plausible value for Ω_p is 38 km/s/kpc. This implies that corotation is at about 4.5 Kpc, slightly beyond the end of the observed bar in the red image. According to the NGC 3783 light distribution, and to its derived rotation curve, a nuclear ring near the ILR should have been formed. This might correspond to the Hα central concentration observed presently (see Fig. 1). But this accumulation should evolve quickly: either a starburst is triggered, that consumes the gas, or the mass concentration is such that a secondary bar can decouple (Friedli & Martinet 1997). A nested bar could take over to drive the gas to the nucleus (Shlosman et al. 1989). It is not possible, with the present spatial resolution, to see any nuclear bar in our red image. The HST image obtained from the archive does not reveal either any smaller structure. Without any faster nuclear bar, the only possibility is that the gas has been driven inwards through a small leading spiral (e.g. Combes 1998). This is a very transient mechanism, which would have disappeared by now.

5. Summary

We present the spatial distribution and kinematics of the neutral atomic hydrogen gas in the galaxy NGC 3783. Our main results are:

- Less than 2% of the total observed HI mass is in the stellar bar (inside a radius of 18″). The total HI mass is found to be $M_{\rm HI} = 1.1 \times 10^9$ M$_\odot$.
- Although the HI spatial distribution appears perturbed, the HI kinematics indicates that most of the gas is in an almost face on distribution (with inclination to the line of sight at $i \approx 25°$), and with the kinematic major axis at $PA \approx 145°$.
- The observed velocity field indicates that HI in NGC 3783 is in differential rotation in a disk with a systemic velocity of $v_{\rm sys} \approx 2910$ km s^{-1} and the north east region being closer to the observer.
- The rotation curve is flat up to 180″ from the nucleus.
- Small velocity deviations of the order of 20 km s^{-1} are observed but they may well be the result of local turbulence, since there are no optical signs of tidal interaction or merger event.
- The HI spatial distribution indicates that gas can be found at large radii in three quadrants, NW, NE and SE. Gas in the SW quadrant is found only at smaller radii.
- If corotation occurs approximately at 1.3 times the radius of the stellar bar, i.e. 24”, as suggested by numerical simulations, then the pattern speed of the bar is estimated to be $\Omega_{\rm b} \approx 38$ km s^{-1} kpc^{-1} and the bright HII regions would indicate density enhancements near the ultra-harmonic resonance (UHR). The model also predicts the existence of a nuclear ring at 750 pc, where an Hα concentration is observed, indeed.

Acknowledgements. We acknowledge helpful comments and suggestions by Tom Jones. JAG-B acknowledges partial financial support from DGAPA-UNAM (Mexico) and from CONACYT (Mexico) that allowed him to spend his sabbatical year at the Department of Astronomy at the University of Minnesota. JAG-B would like to thank the hospitality of the Department of Astronomy at the University of Minnesota, where most of the analysis was done and the first versions of the paper was written and specially John Dickey for his help and useful comments about this work. The work of JF was partially supported by a DGAPA (UNAM) grant, CONACYT (Mexico) grants 400354-5-4843E and 400354-5-0639PE, and by a R&D CRAY Research grant. This research has made use of the NASA/IPAC extragalactic database (NED) which is operated by the Jet Propulsion Laboratory, Caltech, under contract with the National Aeronautics and Space Administration.

References

Alloin D., Santos-Ileo M., Peterson B.M., et al., 1995, A&A 293, 293
Athanassoula E., 1992, MNRAS 259, 345
Atwood B., Baldwin J.A., Carswell R.F. 1982, ApJ 257, 559
Baum S.A., O'Dea C.P., Dallacassa D., de Bruyn A.G., Pedlar A., 1993, ApJ 419, 553
Combes F., 1988, In: Pudritz R.E., Fich M. (eds.) Galactic and Extragalactic Star Formation. Kluwer, p. 475
Combes F., Gerin M., 1985, A&A 150, 327
Combes F., 1998, In: Guiderdoni B., Khembavi A. (eds.) Starbursts: triggers, nature an evolution. Les Houches Lectures, Springer, p. 175
de Bruyn A.G.,, Wilson A.S., 1978, A&A 64, 433
Dultzin-Hacyan D., 1997, Rev. Mex. Astron. Astrofis. Conf. S. 6, 132
Evans I.N., 1988, ApJS 67, 373
Fabbiano G., Gioia I.M., Trinchieri G., 1989, ApJ 347, 127
Fabbiano G., Kim D.-W.,, Trinchieri G., 1992, ApJS 80, 531

Forte J., Vega E.I., Calderon J.H., Feinstein F., 1987, AJ 92, 301
Friedli D., Benz W., 1993, A&A 268, 65
Friedli D., Martinet L., 1997, In: Franco J., Terlevich R., Serrano A. (eds.) Starburst Activity in Galaxies. Rev. Mex. Astron. Astrofis. Conf. Ser. 6, 177
García-Barreto J.A., Franco J., Carrillo R., Venegas S., Escalante-Ramirez B., 1996, Rev. Mex. Astron. Astrofis. 32, 89
García-Burillo S., Sempere M.J., Combes F., 1994, A&A 287, 419
García-Burillo S., Combes F., Gerin M., 1993, A&A 274, 148
George I.M., Turner T.J., Netzer H., 1995, ApJ 438, L67
Giovanelli R., Haynes M.P., 1988, In: Verschuur G.L., Kellermann K.I. (eds.) Galactic and Extragalactic Radio Astronomy. Springer, New York, p. 522
Habe A., Wada K., 1993, In: Franco J., Ferrini F., Tenorio-Tagle G. (eds.) Star Formation, Galaxies and the Interstellar Medium. Cambridge Univ. Press, Cambridge, p. 134
Helou G., Soifer B.T., Rowan-Robinson M., 1985, ApJ 298, L7
Horellou C., Combes F., 1993, In: Combes F., Athanassoula E. (eds.) N body Problems and Gravitational Dynamics. Aussois, Haute Maurienne, France, p. 168
Huchtmeier W.K.,, Richter O-G., 1989, In: A General Catalog of HI Observations of Galaxies. Springer Verlag, New York
Kennicutt R.C., 1981, AJ 86, 1847
Kritsuk A.G., 1983, Astrofisika 19, 263
Lindblad P.A.B., Kristen H., 1996, A&A 313, 733
Lindblad P.A.B., Lindblad P.O., Athanassoula E., 1996, In: Sandqvist Aa., Lindblad P.O. (eds.) Lecture Notes in Physics Vol. 474, Springer Verlag, Berlin, 83
Lynden-Bell D., Kalnajs A.J., 1972, MNRAS 157, 1
Lynden-Bell D., Pringle J.E., 1974, MNRAS 168, 603
Mulchaey J.S., Regan M., Kundu A., 1997, ApJS 110, 299
Noguchi M., 1988, A&A 203, 259
Pelat D., Alloin D., Fosbury R.A.E., 1981, MNRAS 195, 787
Phinney E.S., 1994, In: Shlosman I. (ed.) Mass Transfer Induced Activity in Galaxies. Cambridge Univ. Press, Cambridge, p. 1
Piccinotti G., Mushotzky R.F., Boldt E.A., et al., 1982, ApJ 253, 485
Reichert G.A., Rodríguez-Paswal P.M., Alloin D., et al., 1994, ApJ 425, 582
Salo H., 1991, A&A 243, 118
Sellwood J. A., Debattista V.P., 1996, In: Sandqvist A., Lindblad P.O. (eds.) Barred Galaxies and Circumnuclear Activity.Lecture Notes in Physics Vol. 474, Springer, Berlin, p. 43
Sempere M.J., García–Burillo S., Combes F., Knapen J.H., 1995, A&A 296, 45
Shlosman I., Frank J., Begelman M.C., 1989, Nat 338, 45
Simkin S.M., van Gorkom J., 1984, BAAS 16, 539
Simkin S.M., Su H.J.,, Schwarz M.P., 1980, ApJ 237, 404
Stirpe G.M., Winge C., Altieri B., et al., 1994, ApJ 425, 609
Terlevich R., Tenorio-Tagle G., Franco J., Melnick J., 1992, MNRAS 255, 713
Terlevich R., Tenorio-Tagle G., Franco J., Rozyckza M., 1994, MNRAS 272, 192
Toomre A., 1978, In: Longair M.S., Einasto J. (eds.) The Large Scale Structure of the Universe. IAU Symposium No. 79, Reidel, Dordrecht, p. 109
Tully B.R., 1988, In: Nearby Galaxies Catalog. Cambridge Univ. Press, Cambridge
Ulvestad J.S.,, Wilson A.S., 1984, ApJ 285, 439
Ulvestad J.S., Wilson A.S., Sramek R.A., 1981, ApJ 247, 419
Winge C., Pastoriza M. G., Storchi-Bergmann T., Lipari S., 1992, ApJ 393, 98